DOI 10.47176/sjis.8.2.10

Original Article

SRPH

SJIS, 2022; 8(2): 10-21

Application of RCS and GRM Techniques for Depth Estimation of Refractor Interfaces in Civil Engineering Projects

Hossein Azimzadeh[1], Fatemeh Bozorgi[2,*]

[1,2] Institute of Geophysics, University of Tehran, Iran.

***Corresponding Author:**

bozorgi.fatemeh@gmail.com

Received: 07 April, 2026
Received: 15 May, 2026
Accepted: 20 June, 2026
Published: 25 June, 2026

ABSTRACT

Seismology, a branch of geophysics, has seen significant advancements since its inception. Among the various techniques developed, the seismic refraction method is an essential tool for subsurface exploration. This method relies on the principles of wave propagation to reveal geological structures, making it vital for a range of applications such as resource exploration, environmental assessments, and civil engineering projects. In seismic refraction studies, methods that calculate the depth of the refractor interface at each geophone location offer substantial benefits. Various techniques have been developed for interpreting seismic refraction data. This research presents a case study that employs the RCS and GRM methods on seismic refraction data collected from a civil engineering project in Tehran. To implement these methods, all steps associated with the GRM method were executed using Excel. This analysis involved calculating velocity function values and time-depth relationships based on the arrival times of both forward and reverse shots at the geophone locations along the seismic refraction profile. Additionally, the RCS method, known for its simplicity and efficiency in processing full trace data through the convolution of forward and reverse shot records, was performed using MATLAB and SeisImager software. The results from both methods provided insights into the depth of the refractor interface along the surveyed profile.

Keywords: Refraction Seismic, Generalized Reciprocal Method, Refraction Convolution Section

Introduction

Among all geophysical exploration techniques, seismic surveying is particularly significant, primarily due to its ability to identify subsurface features ranging from large to small scales. In simple terms, seismic methods involve the assessment of the shapes and physical properties of the Earth's subsurface layers based on the returns of sound waves that are propagated through the Earth [1-4]. The method relies on the principle that seismic waves travel at different velocities through various geological materials, allowing for the identification of subsurface layers based on the refraction of these waves at interfaces [5]. In general, two types of seismic method are common: reflection and refraction. Utilizing refraction traveltime data for imaging the subsurface has long been a standard technique. This technique is attractive due to its cost-effective field operations and the straightforward interpretation of the results [5,6]. The seismic refraction method plays a crucial role in subsurface exploration, particularly in civil engineering projects where understanding the depth of refractor interfaces is essential. This method provides insights into various geological and petrophysical characteristics, such as rock type, porosity, weathering, joints, water saturation, and elasticity [7]. In civil engineering, understanding the depth and nature of refractor interfaces is critical for several reasons. For instance, the identification of bedrock depth is crucial for the foundation design, while detecting anomalies can inform hazard assessments and mitigation strategies [8].

Recent innovations in seismic refraction techniques have significantly enhanced our ability to analyze shallow subsurface structures. Among these advancements, the Generalized Reciprocal Method (GRM), introduced by [7], is particularly noteworthy. The GRM can effectively

[Downloaded from sjis.srpub.org on 2026-11-21]

[DOI: 10.47176/sjis.8.2.10]

CC BY NC

Publisher: Scientific Research Publishing House (SRPH), Shirvan, Iran
http://srpub.org
Email: sjis@srpub.org

define layers with varying thicknesses and seismic velocities, representing a significant improvement over traditional methods [9]. Unlike conventional approaches, the GRM leverages both forward and reverse arrival times, which makes it less sensitive to dip angles of up to around 20 degrees. This feature is especially beneficial for accurately calculating depths to undulating refractors, especially when overlying strata exhibit velocity gradients. Additionally, the GRM accommodates irregular layers, thereby improving our understanding of complex geological formations [7].

Building on the foundation established by the GRM, the introduction of the Refraction Convolution Section (RCS) method marks another significant advancement forward in processing shallow seismic refraction data. This method is notable for its simplicity and efficiency, generating time cross-sections that closely resemble traditional reflection cross-sections. By convolving seismic records from forward and reverse shots, the RCS not only enhances the signal-to-noise ratios but also provides a clear picture of the depth to the refractor interface [10]. This approach effectively compensates for the effects of geometrical spreading, yielding more accurate geological interpretations.

In this study, we analyze seismic refraction data obtained from a civil engineering project in Tehran using both the RCS and GRM methods. Our goal is to demonstrate the effectiveness of these techniques in reconstructing refractor interfaces and gaining valuable insights into subsurface structures. Using the GRM approach, we calculated velocity functions and time-depth relationships based on arrival traveltimes recorded at various geophone locations along the seismic profile. Meanwhile, the RCS method was employed to process the full seismic trace, allowing for a comprehensive examination of the collected data. Through this research, we aim to showcase the benefits of combining the RCS and GRM methodologies, highlighting their potential to enhance subsurface exploration techniques. By analyzing seismic profiles and applying these advanced processing methods, we hope to contribute to the ongoing development of geophysical techniques, ultimately enriching our understanding of complex geological environments.

Field Data

This study involved the acquisition of three seismic refraction profiles. Profile 1 was not usable due to the absence of a reverse shot and the overall poor quality of the collected data. Therefore, data from Profile 3 was selected for analysis, based on evaluations of Profiles 2 and 3. Profile 3 has a total length of 23 meters, with geophones placed at one-meter intervals. Data collection was performed using a 24-channel system. The recordings have a duration of 128 milliseconds and a sampling rate of 0.25 milliseconds, resulting in 512 samples recorded for each trace. In total, seven shots were executed for the profile under study, with the records from both the forward and reverse shots illustrated in Figures 1 and 2.

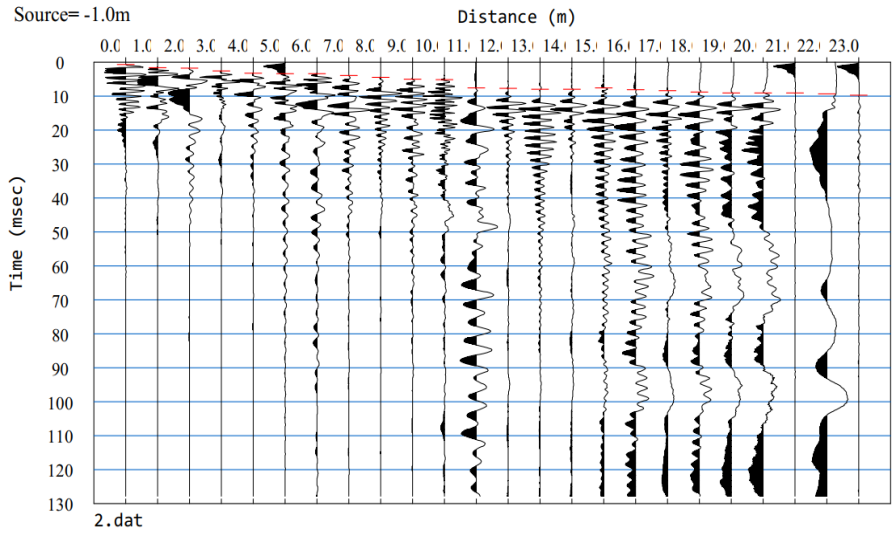


Fig. 1. Seismic refraction data related to the forward shot of profile number 3**.**

[Downloaded from sjis.srpub.org on 2026-11-21]

[DOI: 10.47176/sjis.8.2.10]

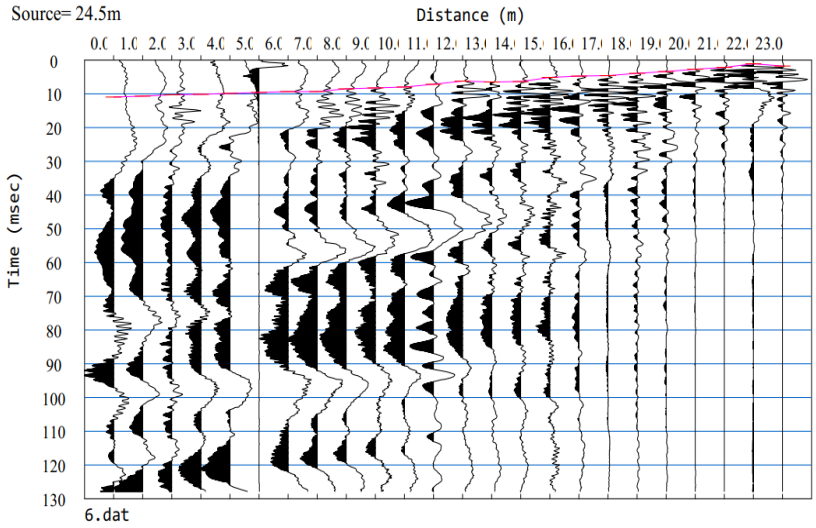


Fig. 2. Seismic refraction data related to the final shot of profile number 3.

Methods

RCS Method

The RCS method involves performing convolution between the traces from the forward shot and those from the reverse shot. This process generates a convolutional section that represents changes in the depth of the refractor interface. A key distinction of the RCS method, compared to other techniques, is its reliance on the amplitudes of refraction waves. In contrast, methods such as delay time, Plus-Minus, and GRM use arrival traveltimes to analyze wave velocities and calculate the thickness of geological layers.

Amplitude Diminution with Offset

As seismic waves propagate through the ground, their amplitudes diminish with increasing offset due to geometrical spreading. This phenomenon can be quantified and can range between 1/X^2 and 1/X^3 , where X represents the distance. The reduction in amplitude due to geometrical spreading is a fundamental aspect of wave propagation in the earth; in seismology, all data reflect the influence of geometrical spreading. In this study, we examined the issue of amplitude reduction with increasing distance using data from Profile 3. The results of this analysis are presented in Figures 3 and 4. It is worth mentioning that the figures display the amplitudes corresponding to the first troughs from the seismic traces, which have been normalized to values between zero and one. As shown, the amplitude reduction curves in both cases closely follow the trend of $1/X^2$. The blue curve indicates a scenario where the upper limit of normalization is set to a maximum value of $1/X^2$, while the green curve represents a scenario where the upper limit of normalization is set to a maximum value of $1/X^3$.

Convolution of Forward and Reverse Shots

The Z-transform relationship for a trace corresponding to the initial shot can be expressed using Equation 1, while the Z-transform for a trace related to the final shot is detailed in Equation 2.

$$F(z) = f_m z^m + f_{m+1} z^{m+1} + f_{m+2} z^{m+2} + \cdots \quad (1)$$
where $f_j = 0$ for $j < m$,

$$R(z) = r_n z^n + r_{n+1} r^{n+1} + r_{n+2} z^{n+2} + \cdots \quad (2)$$
where $r_j = 0$ for $j < n$.

In these equations, the values f_m , f_{m+1}, … in Equation 1 represent the amplitude values at each time sample, and the values r_n , r_{n+1},… in Equation 2 denote the corresponding amplitude values for the reverse shot. Equation 3 illustrates the convolution in the Z-transform domain, which simplifies to a conventional multiplication operation.

$$F(z) * R(z) = f_m r_n z^{m+n} + (f_m r_{n+1} + f_{m+1} r_n) z^{m+n+1} + (f_m r_{n+2} + f_{m+1} r_{n+1} + f_{m+2} r_n) z^{m+n+2} + \cdots \quad (3)$$

Focusing on the sum $m + n$, we see that it is equivalent to $t_{forward} + t_{reverse}$ as shown in Equation 4, a relationship referred to as Time-Depth in the GRM method.

$$Time - Depth = (t_{forward} + t_{reverse} - t_{reciprocal})/2, \quad (4)$$

[Downloaded from sjis.srpub.org on 2026-11-21]

[DOI: 10.47176/sjis.8.2.10]

Since the numerical value of $t_{reciprocal}$ is constant throughout the project, we can perform convolution between the traces from the forward and reverse shots. Knowing the value of $t_{reciprocal}$, enables us to derive the Time-Depth profile without manually picking data in the field. This approach allows for straightforward generation of the Time-Depth Profile through convolution. These steps were applied to the data from profile 3, and the resulting outcomes are presented in Figure 5.

Calculation of Interval Velocity for the First Layer

Table 1 presents the peaked arrival traveltimes for each trace across various shots. Out of the seven shots conducted for this profile, one shot at an offset of 24.5 meters was repeated due to a delay in data acquisition. Furthermore, the offset shot taken at a 10-meter offset was excluded from picking due to weak source energy and a low signal-to-noise ratio (SNR). Consequently, out of the five picked shots, two were forward and reverse shots, along with three interior shots that were included in the analysis. Interior shots provide data redundancy and improve near-surface velocity estimation. Figure 6 displays the corresponding time-distance curves.

Utilizing the recorded time-distance curves, we can derive four velocity intervals for the first layer, labeled A, B, C, and D in Figure 7.

By calculating the slope of the best-fit line for the time-distance graph at each shot location for the direct waves, we can determine the velocity of the first layer. With these velocities, we can subsequently compute the interval velocities for the specified sections as outlined below:

$$\overline{V_{1A}} = \frac{V_{R1} + V_{L2}}{2} = \frac{1794 + 1446}{2} = 1620\, m/s \quad (5)$$

$$\overline{V_{1B}} = \frac{V_{R2} + V_{L3}}{2} = \frac{1389 + 2049}{2} = 1719\, m/s \quad (6)$$

$$\overline{V_{1C}} = \frac{V_{R3} + V_{L4}}{2} = \frac{2005 + 2047}{2} = 2026\, m/s \quad (7)$$

$$\overline{V_{1D}} = \frac{V_{R4} + V_{L5}}{2} = \frac{2215 + 1826}{2} = 2020\, m/s \quad (8)$$

GRM Method

Determining the Acceptable Range for Implementing the GRM Method

The GRM method can only be applied within the overlapping range of refraction wave arrivals from the forward and reverse shots of the seismic profile. Therefore, based on the time-distance graphs for the forward and reverse shots, we can identify the relevant overlapping window.

As shown in Figure 8, the refraction wave was received from the 6th geophone for the forward shot of the profile, while for the reverse shot, the wave was recorded from the 18th geophone onward. Using these two data points, we can determine the acceptable range for implementing the GRM method, represented by the yellow box in Figure 8.

Calculation of T_V

The first step in the GRM method is velocity analysis, achieved by calculating the Velocity analysis function (T_V). The formula for T_V is similar to the T^- equation used in the Plus-Minus method, as both methods rely on velocity analysis. In the T_V formula, the values T_{AY}, T_{BX} , and T_{AB} are obtained from the time-distance graph based on the arrival traveltimes at the geophones (Figure 9).

To calculate T_V, we utilize Equation 5.

$$T_V = \frac{T_{AY} - T_{BX} + T_{AB}}{2} \quad (5)$$

To compute the reciprocal time, if there are layers with slopes between 5 to 10 degrees, this value will be approximately the same for both the right and left shots in the profile. However, if there is a slight discrepancy, we can calculate and use the average of both sides. For this dataset, we utilized an average value of 10 milliseconds. For velocity analysis, we seek an optimal distance xy. This distance xy should maximize the likelihood of returning rays detected at the surface from a point on the refractor interface that has a critical refraction angle. To determine this optimal xy, we will evaluate several different xy distances, calculate their corresponding T_V values, and plot these values against Offset AG. This will allow us to identify the optimal xy. The Offset AG represents the distance from the source to point G, which is located exactly at the center of the xy distance. In the GRM method, the minimum xy distance occurs when both receivers are positioned next to each other, while the maximum xy distance occurs when each receiver is placed at opposite sides of the yellow window. In Figure 9, the line GH represents an imaginary vertical line on the interface between the two layers. When xy are very close together, it appears as if they are both positioned at point G. However, as the distance between these two points increases, the angle between xy at point H changes. Our objective is to find the xy distance at which the refracted ray falls exactly on the sides XH and YH of triangle XHY, or equivalently, the angle bisector between XH and YH equals the critical angle.

[Downloaded from sjis.srpub.org on 2026-11-21]

[DOI: 10.47176/sjis.8.2.10]

To begin, we will select a specific Offset AG and start with a distance of Δx = 1 m, incrementally increasing this distance by constant factors. We will repeat this process for various Offset AG values. Eventually, we will plot the Offset AG values versus the T_V values obtained for the different xy distances (Figure 10). By evaluating the smoothness of the resulting graphs, we can determine the optimal xy. Specifically, we will identify the xy distance for which the coefficient of determination (R^2) of the linear regression is closest to 1; this value will be considered the optimal xy and used in the subsequent calculations of T_G .

Calculation of T_G

By determining the optimal xy using the T_V versus Offset AG graph, the slope of the related graph will yield the apparent velocity of the second layer (V'), which we will then use to calculate the average velocity ($\bar{V}$). Based on the data analysis according to the aforementioned process, the determined optimal xy for this dataset is 4 meters.

By determining the optimal xy and V', we will be able to calculate the value of T_G using Equation 6.

$$T_G = \frac{T_{AY} + T_{BX} - T_{AB} - (\frac{XY}{V'})}{2} \quad (6)$$

Calculating T_G for various xy values, along with the corresponding V', will allow us to plot the T_G versus Offset AG graph. This process will ultimately lead to a better selection of the optimal xy. In the T_G-Offset AG graph, we will choose the plot that exhibits the greatest irregularity. This choice is based on the fact that the T_G relationship is a function of time and depth; the greater the distortions are, the better we can identify the geometrical changes of the refractor interface.

It is essential to consider both the $T_V - \text{Offset AG}$ and $T_G - \text{Offset AG}$ graphs when selecting the optimal xy. The optimal xy identified in both graphs should be consistent and meet the specified conditions to validate each other. As illustrated in Figure 11, the minimum R^2 value corresponds to xy= 4, which is consistent with the optimal xy determined in the $T_V - \text{Offset AG}$ graph.

Calculation of Average Velocity ($\bar{V}$) and Depth (h)

Using the values of T_G, V', and the optimal xy obtained through the velocity analysis and the methods outlined above, we can calculate the average velocity ($\bar{V}$) using Equation 7.

$$\bar{V} = \sqrt{\frac{V'^2 XY}{XY + 2T_G V'}} \quad (7)$$

After computing $\bar{V}$, along with the values of T_G and V', we can determine the thickness of the first layer using Equation 8.

$$h = \frac{T_G \bar{V} V'}{\sqrt{V'^2 - \bar{V}^2}} \quad (8)$$

The results of these calculations and analyses are presented in Tables 2 and 3.

Cross-Sectional Representation of the Subsurface Based on the Calculated Thickness

After completing the relevant calculations, we can determine the thickness of the first layer beneath each geophone. Using the elevation coordinates of the geophone locations, we can create a cross-sectional profile of the subsurface along the survey line. This profile will provide insights into the actual geometry of the fracture surface and the positioning of the underlying layers.

Figure 12 displays the cross-section obtained using the GRM method, while Table 4 presents the calculated elevation values for the refractor interface along Profile 3.

Conclusion

As demonstrated in Figure 5, we initially applied the RCS method to convolve the seismic responses from both the forward and reverse shots. Afterward, we shifted all traces by the calculated value of $t_{reciprocal}$. By picking the arrival traveltimes on the resulting convolved traces, we estimated the depth and geometry of the refractor interface, which closely aligns with the geometrical representation obtained from the GRM method (Figure 12).

The cross-section derived from the convolution is free from the effects of geometrical spreading, allowing for interpretable amplitude information. By analyzing the amplitudes of the first troughs and plotting them, we can perform an amplitude inversion.

Using the GRM method, we conducted a velocity analysis to determine the velocities of the first and second layers, utilizing the $T_v - \text{Offset AG}$ and $T_G - \text{Offset AG}$ graphs. After identifying the optimal xy values, we then calculated the thickness of the first layer by employing the apparent velocities (V') and the average velocity ($\bar{V}$) of the second layer. Finally, we calculated the depth of the refractor interface using the corresponding equations.

[Downloaded from sjis.srpub.org on 2026-11-21]

[DOI: 10.47176/sjis.8.2.10]

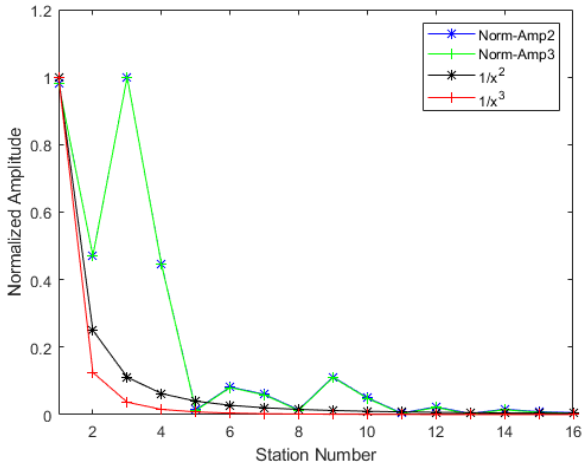


Fig. 3. Effect of geometrical spreading on the amplitudes of first-arrival traveltimes in the seismic refraction data from the forward shot.

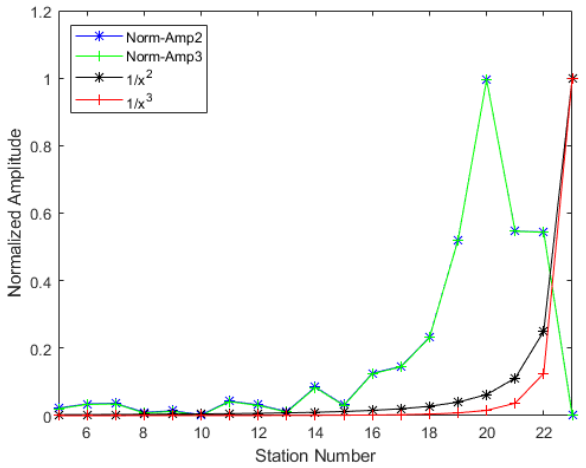


Fig. 4. Effect of geometrical spreading on the amplitudes of first-arrival traveltimes in the seismic refraction data from the reverse shot.

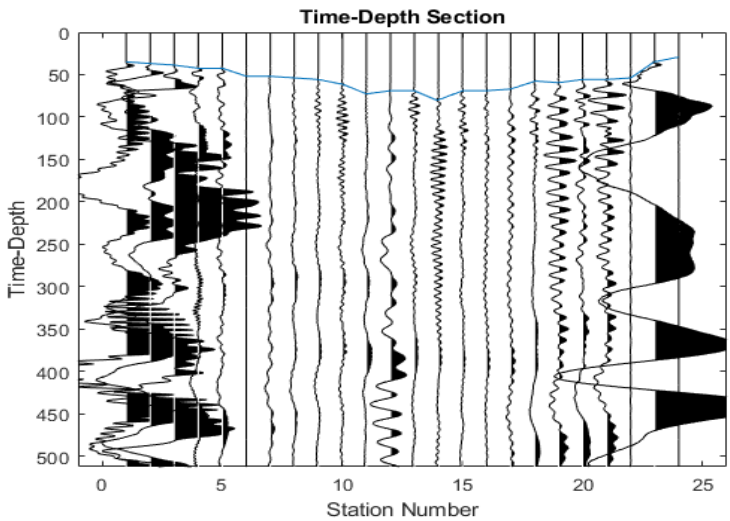


Fig. 5 .convolution section obtained from the traces

[Downloaded from sjis.srpub.org on 2026-11-21]

[DOI: 10.47176/sjis.8.2.10]

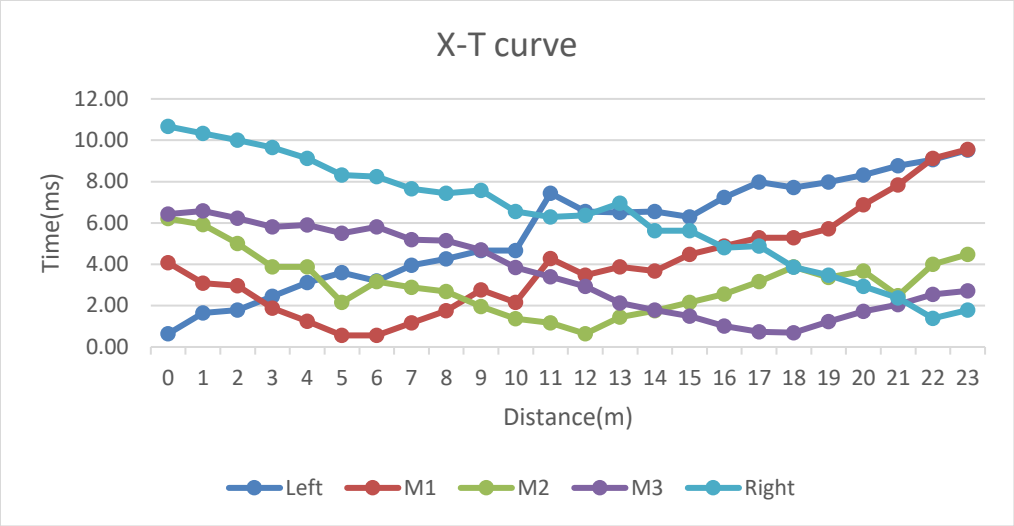


Fig. 6 . Time-distance curves for profile number 3

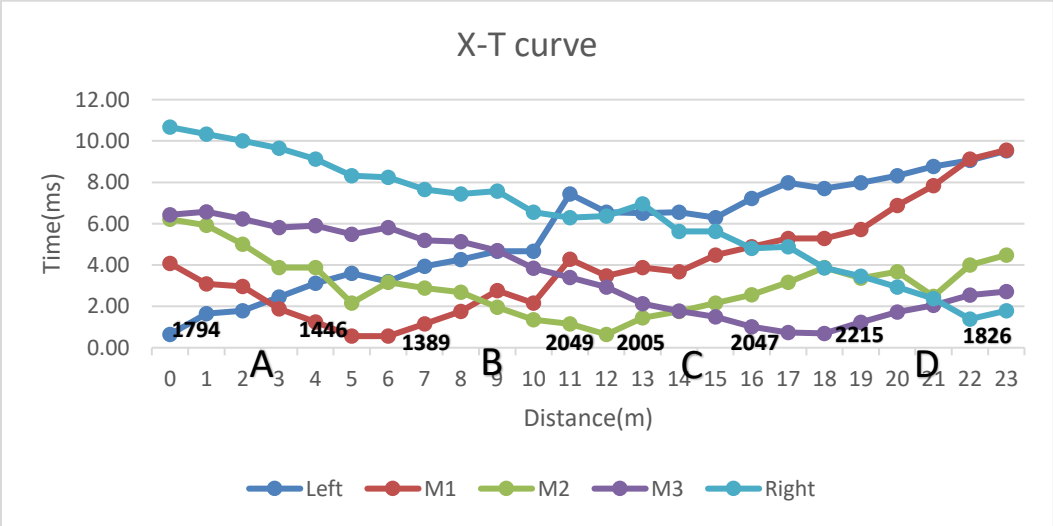


Fig. 7 . Interval velocity for the first layer (V1)

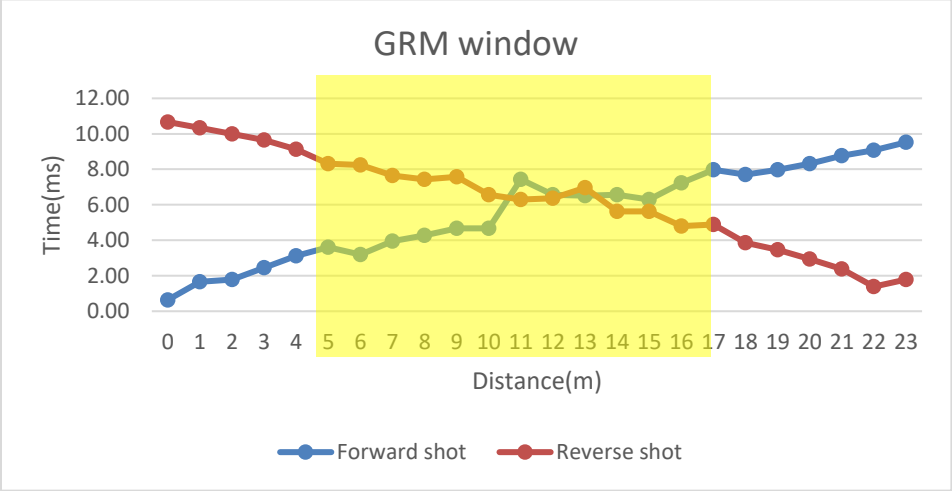


Fig. 8. Acceptable range for implementing the GRM method.

[Downloaded from sjis.srpub.org on 2026-11-21]

[DOI: 10.47176/sjis.8.2.10]

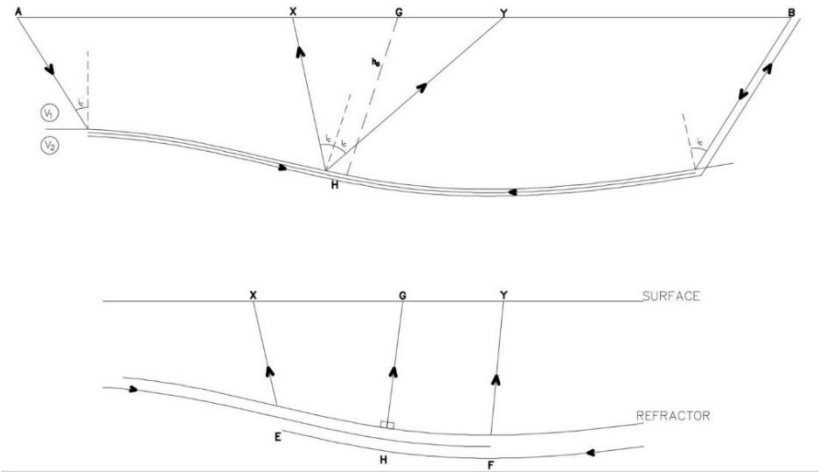


Fig. 9. Schematic representation of the positions of points in the GRM method.

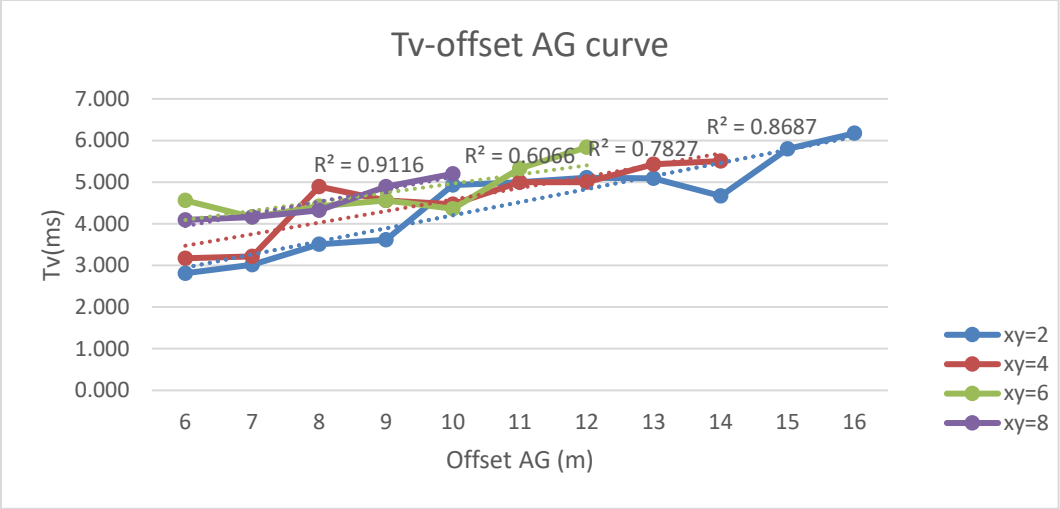


Fig. 10. T_V – Offset AG graph

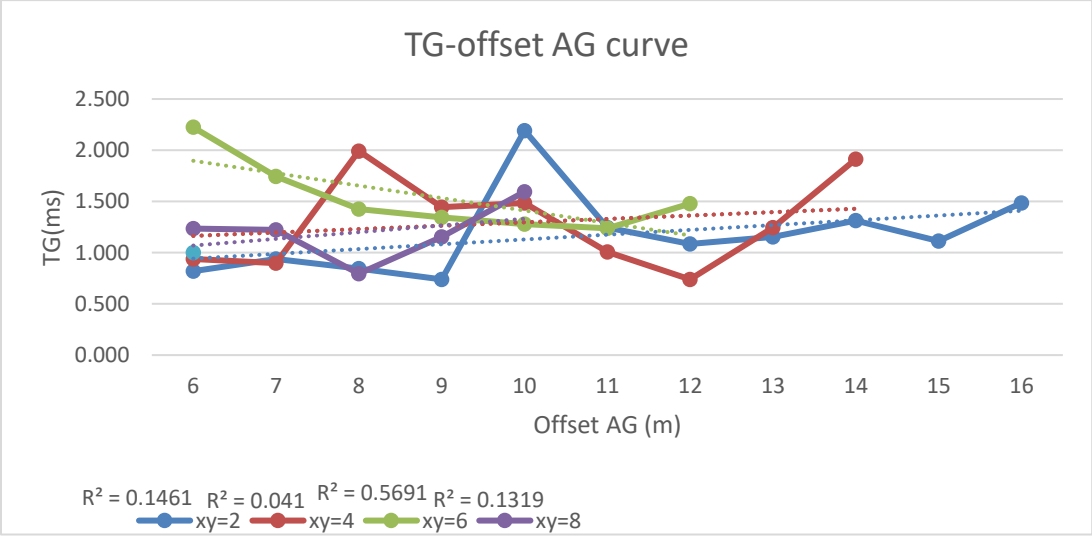


Fig. 11. T_G – Offset AG graph

[Downloaded from sjis.srpub.org on 2026-11-21]

[DOI: 10.47176/sjis.8.2.10]

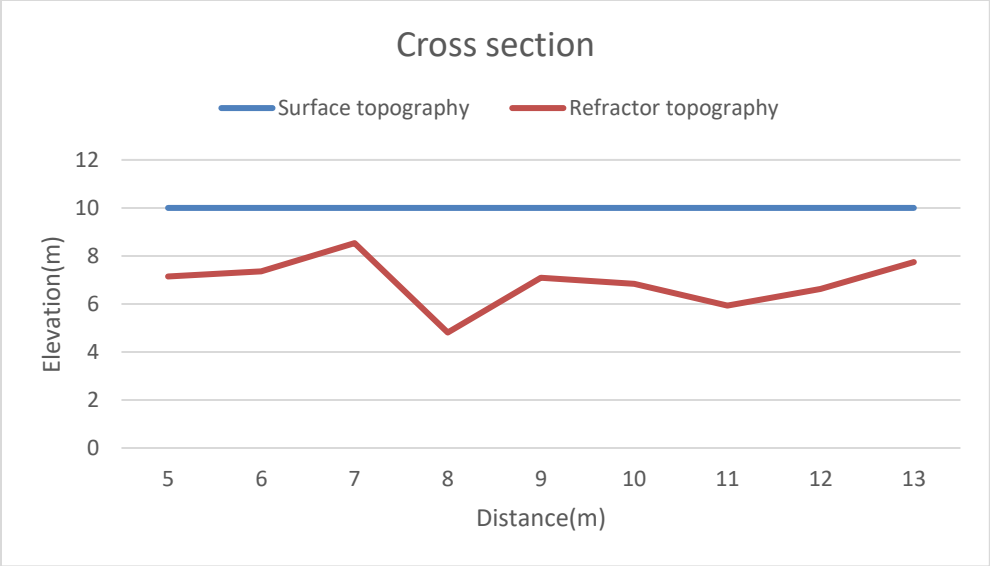


Fig. 12. Subsurface layering, thickness, and depth of the refractor interface beneath each geophone

Table 1 .Peaked arrival traveltimes for the executed shots (M1:M3 are interior shots).

X(m)		Left(ms)	M1(ms)	M2(ms)	M3(ms)	Right(ms)
0		0.64	4.08	6.21	6.44	10.67
1		1.65	3.08	5.92	6.58	10.33
2		1.79	2.96	5.00	6.22	10.00
3		2.45	1.88	3.88	5.81	9.65
4		3.12	1.24	3.88	5.90	9.12
5		3.60	0.56	2.16	5.49	8.32
6		3.20	0.56	3.16	5.81	8.24
7		3.95	1.16	2.88	5.19	7.65
8		4.27	1.76	2.68	5.14	7.44
9		4.67	2.76	1.96	4.69	7.57
10		4.67	2.16	1.36	3.84	6.56
11		7.44	4.28	1.16	3.40	6.29
12		6.56	3.48	0.64	2.93	6.37
13		6.51	3.88	1.44	2.13	6.96
14		6.56	3.68	1.76	1.78	5.63
15		6.29	4.48	2.16	1.49	5.63
16		7.23	4.88	2.56	1.01	4.80
17		7.97	5.28	3.16	0.73	4.88
18		7.71	5.28	3.88	0.69	3.87
19		7.97	5.72	3.36	1.23	3.47
20		8.32	6.88	3.68	1.72	2.93
21		8.77	7.84	2.48	2.04	2.37
22		9.07	9.12	4.00	2.54	1.39
23		9.52	9.56	4.48	2.72	1.79

[Downloaded from sjis.srpub.org on 2026-11-21]

[DOI: 10.47176/sjis.8.2.10]

Table 2. Values of T_V – Offset AG

-1		24.5		T_recip	AG	TV			
X	**Left Shot**	**X**	**Right Shot**			**XY=2**	**XY=4**	**XY=6**	**XY=8**
0	0.64	0	10.67	10	-	-	-	-	-
1	1.65	1	10.33	10	-	-	-	-	-
2	1.79	2	10.00	10	-	-	-	-	-
3	2.45	3	9.65	10	-	-	-	-	-
4	3.12	4	9.12	10	-	-	-	-	-
5	3.60	5	8.32	10	5	-	-	-	-
6	3.20	6	8.24	10	6	2.813	-	-	-
7	3.95	7	7.65	10	7	3.013	3.173	-	-
8	4.27	8	7.44	10	8	3.507	3.213	4.560	-
9	4.67	9	7.57	10	9	3.613	4.893	4.160	4.093
10	4.67	10	6.56	10	10	4.933	4.560	4.427	4.160
11	7.44	11	6.29	10	11	5.000	4.467	4.560	4.320
12	6.56	12	6.37	10	12	5.107	5.000	4.360	4.893
13	6.51	13	6.96	10	13	5.093	5.000	5.333	5.200
14	6.56	14	5.63	10	14	4.667	5.427	5.840	-
15	6.29	15	5.63	10	15	5.800	5.507	-	-
16	7.23	16	4.80	10	16	6.173	-	-	-
17	7.97	17	4.88	10	17	-	-	-	-
18	7.71	18	3.87	10	-	-	-	-	-
19	7.97	19	3.47	10	-	-	-	-	-
20	8.32	20	2.93	10	-	-	-	-	-
21	8.77	21	2.37	10	-	-	-	-	-
22	9.07	22	1.39	10	-	-	-	-	-
23	9.52	23	1.79	10	-	-	-	-	-

[Downloaded from sjis.srpub.org on 2026-11-21]

[DOI: 10.47176/sjis.8.2.10]

Table 3. Values of $T_G - Offset\ AG0$

-1		24.5		T_recip	AG	TG				V_av(m/ms)	Z(m)
X	**Left Shot**	**X**	**Right Shot**			**XY=2**	**XY=4**	**XY=6**	**XY=8**		
0	0.64	0	10.67	10	-	-	-	-	-	-	-
1	1.65	1	10.33	10	-	-	-	-	-	-	-
2	1.79	2	10.00	10	-	-	-	-	-	-	-
3	2.45	3	9.65	10	-	-	-	-	-	-	-
4	3.12	4	9.12	10	-	-	-	-	-	-	-
5	3.60	5	8.32	10	5	-	-	-	-	-	-
6	3.20	6	8.24	10	6	0.819	-	-	-	-	-
7	3.95	7	7.65	10	7	0.939	0.939	-	-	2.198	2.855
8	4.27	8	7.44	10	8	0.846	0.899	2.224	-	2.229	2.640
9	4.67	9	7.57	10	9	0.739	1.992	1.744	1.235	1.684	1.466
10	4.67	10	6.56	10	10	2.192	1.446	1.424	1.221	1.900	5.191
11	7.44	11	6.29	10	11	1.246	1.486	1.344	0.795	1.881	2.905
12	6.56	12	6.37	10	12	1.086	1.006	1.278	1.155	2.151	3.169
13	6.51	13	6.96	10	13	1.152	0.739	1.238	1.595	2.362	4.063
14	6.56	14	5.63	10	14	1.312	1.246	1.478	-	2.002	3.381
15	6.29	15	5.63	10	15	1.112	1.912	-	-	1.711	2.257
16	7.23	16	4.80	10	16	1.486	-	-	-	-	-
17	7.97	17	4.88	10	17	-	-	-	-	-	-
18	7.71	18	3.87	10	-	-	-	-	-	-	-
19	7.97	19	3.47	10	-	-	-	-	-	-	-
20	8.32	20	2.93	10	-	-	-	-	-	-	-
21	8.77	21	2.37	10	-	-	-	-	-	-	-
22	9.07	22	1.39	10	-	-	-	-	-	-	-
23	9.52	23	1.79	10	-	-	-	-	-	-	-

[Downloaded from sjis.srpub.org on 2026-11-21]

[DOI: 10.47176/sjis.8.2.10]

Table 4. Elevation values of the ground surface and the refractor interface.

X(m)	Left(ms)	M1(ms)	M2(ms)	M3(ms)	Right(ms)
0	0.64	4.08	6.21	6.44	10.67
1	1.65	3.08	5.92	6.58	10.33
2	1.79	2.96	5.00	6.22	10.00
3	2.45	1.88	3.88	5.81	9.65
4	3.12	1.24	3.88	5.90	9.12
5	3.60	0.56	2.16	5.49	8.32
6	3.20	0.56	3.16	5.81	8.24
7	3.95	1.16	2.88	5.19	7.65
8	4.27	1.76	2.68	5.14	7.44
9	4.67	2.76	1.96	4.69	7.57
10	4.67	2.16	1.36	3.84	6.56
11	7.44	4.28	1.16	3.40	6.29
12	6.56	3.48	0.64	2.93	6.37
13	6.51	3.88	1.44	2.13	6.96
14	6.56	3.68	1.76	1.78	5.63
15	6.29	4.48	2.16	1.49	5.63
16	7.23	4.88	2.56	1.01	4.80
17	7.97	5.28	3.16	0.73	4.88
18	7.71	5.28	3.88	0.69	3.87
19	7.97	5.72	3.36	1.23	3.47
20	8.32	6.88	3.68	1.72	2.93
21	8.77	7.84	2.48	2.04	2.37
22	9.07	9.12	4.00	2.54	1.39
23	9.52	9.56	4.48	2.72	1.79

References

1. Telford, W. M., Geldart, L. P., & Sheriff, R. E. (1990). Applied geophysics. Cambridge university press.
2. Sheriff, R. E., & Geldart, L. P. (1995). Exploration seismology. Cambridge university press.
3. Kearey, P., Brooks, M., & Hill, I. (2002). An introduction to geophysical exploration (Vol. 4). John Wiley & Sons.
4. Mondol, N. H. (2015). Seismic exploration. Petroleum Geoscience: From Sedimentary Environments to Rock Physics, 427-454.
5. Green, R. (1974). The seismic refraction method—a review. Geoexploration, 12(4), 259-284.
6. Zhang, J., & Toksöz, M. N. (1998). Nonlinear refraction traveltime tomography. Geophysics, 63(5), 1726-1737.
7. Palmer, D. (1980). The generalized reciprocal method of seismic refraction interpretation: Soc. Expl. Geophys.
8. Davis, J. L., & ANNAN, A. P. (1989). Ground-penetrating radar for high-resolution mapping of soil and rock stratigraphy 1. Geophysical prospecting, 37(5), 531-551.
9. Kilty, K. T., Norris, R. A., McLamore, W. R., Hennon, K. P., & Euge, K. (1986). Seismic refraction at Horse Mesa Dam: An application of the generalized reciprocal method. Geophysics, 51(2), 266-275.
10. Palmer, D. (2005). Digital processing of shallow seismic refraction data with the refraction convolution section. University of New South Wales (Australia).

SJIS

Copyright: © 2026 The Author(s); This is an open-access article distributed under the terms of the Creative Commons Attribution License (http://creativecommons.org/licenses/by/4.0), which permits unrestricted use, distribution, and reproduction in any medium, provided the original work is properly cited.

Citation: Azimzadeh H, Bozorgi F. Application of RCS and GRM Techniques for Depth Estimation of Refractor Interfaces in Civil Engineering Projects. SJIS, 2022; 8(2): 10-21.
https://doi.org/10.47176/sjis.8.2.10

[Downloaded from sjis.srpub.org on 2026-11-21]

[DOI: 10.47176/sjis.8.2.10]